DOUBLY-FED INDUCTION MACHINE IN WIND POWER GENERATION

Hector A. Pulgar-Painemal, Peter W. Sauer
University of Illinois at Urbana-Champaign

Abstract: This paper presents the steady-state model of a variable-speed wind power machine based on a doubly-fed induction generator (DFIG). Using a fifth order dynamic model of an induction machine, a modified equivalent circuit is derived. It uses the synchronously rotating reference frame in which the q-axis leads the d-axis by ninety degrees. In addition, the relationships between power and rotor-voltages are studied. A strong coupling in the q-axis rotor voltage and active power as well as the d-axis rotor voltage and reactive power is observed. These couplings are analyzed and the ability of the DFIG to produce reactive power is studied. Finally, the power capability characteristic of the machine is described which shows similarities to the capability curve of conventional synchronous generators. Considering the maximum rotor current, the boundary of a safe operation is best described by an elliptical region in the complex power plane. In addition, considering the limits of maximum rotor voltage, stator current and maximum active power the well-known D-curve or capability chart is obtained.

Key Words: Wind Power Modeling, Power Systems, Steady-State Model, Capability Curve

I. INTRODUCTION

In the 1990s, wind power turbines were characterized by a fixed-speed operation. Basically, they consisted of the coupling of a wind turbine, a gearbox and an induction machine directly connected to the grid. Additionally, they used a soft starter to energize the machine and a bank of capacitors to compensate the machine power reactive absorption. Although being simple, reliable and robust, the fixed-speed wind turbines were inefficient and power fluctuations were transmitted to the network due to wind speed fluctuations [1].

In the mid-1990s, variable-speed wind power turbines gave an impulse to the wind power industry. A better turbine control reduces power fluctuations. In addition, optimal power extraction from wind was possible by operating the turbine at optimal speed. Among the different configurations of variable-speed wind power turbines, the doubly-fed induction generator, at present, is the most used in the development of wind farm projects. This configuration consists of the coupling of a turbine, a gearbox and an induction machine doubly connected to the grid—directly connected from the stator circuits and indirectly connected from the rotor circuits by using converters. Its main drawbacks are the use of slip rings and protection in case of grid disturbances [2]. The control is done by (a) controlling the voltage applied to the rotor circuits, (b) by adjusting the pitch angle of the turbine blades (angle of incidence of the blade and the wind direction), and (c) by designing aerodynamically the turbine blades to stall when the wind speed exceed a predefined limit—stall control [3].

This paper studies the DFIG used in variable-speed wind power generation. Using a fifth order dynamic model of an induction machine, a modified equivalent circuit is derived. Using a synchronously rotating reference frame, the incidence of the applied rotor-voltages in the machine operation is studied. Moreover, the DFIG's ability to produce reactive-power is analyzed. Finally, the power capability characteristic of the machine is described which shows similarities to the capability curve of conventional synchronous generators.

This paper is structured as follow. In Section II a general description of wind power generation is given. In Section III machine models and curve-characteristics are shown. Finally, in Section IV conclusions are presented.

II. WIND POWER GENERATION PRINCIPLES

During the last years, the most used configuration in wind power projects has been the doubly-fed induction generator. In the literature, this configuration is known as Type C which is shown in Figure 1. The main advantage of this configuration is that it allows variable-speed operation. Therefore, the power extraction from the wind can be optimized. The converters feed the low-frequency rotor circuits from the grid. The converters are partially scaled requiring a rated power of about 30% of the generator rating. Usually, the slip varies between 40% at sub-synchronous speed and -30% at super-synchronous speed [2].

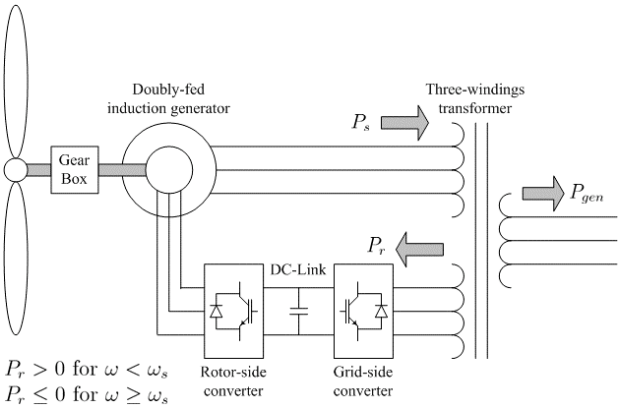

Figure 1. Type C Wind Turbine configuration.

Typically, the grid-side converter is controlled to have a unity power factor and a constant voltage at the *DC*-link. The rotor-side converter is usually controlled to have (a) optimal power extraction from the wind and (b) a specified reactive power at the generator terminal. Note that this converter provides sinusoidal three-phase voltages at the slip frequency. Therefore, assuming that the converters are lossless, the net power injected by the generator to the grid is

$$P_{gen} = P_s - P_r \tag{1}$$

$$Q_{gen} = Q_s \tag{2}$$

where P_s and Q_s are the active and reactive power going out of the stator. P_r is the active power injected by the rotor-side converter to the rotor circuit.

In 1920, Albert Betz, a German pioneer of wind power technology, studied the best utilization of wind energy in wind mills establishing a theoretical limit for the power extraction. Basically, it said that independently of the turbine design, at most $\frac{16}{27} \approx 0.593$ of the wind kinetic energy can be converted into mechanical energy [2]. The energy conversion in wind turbines are based on drag or lift forces. While old wind turbines were mainly based on drag forces, e.g., Savonius design, modern wind turbines are mainly based on lift forces. The air flow in modern turbines creates a pressure difference on the blade tips causing a lift force—similar to the lift force created on an airplane's wings.

In order to understand the power extraction from the wind, it is required to define the *tip speed ratio*, λ, which is the ratio between the speed of a blade tip v_{tip} $[m/s]$ and the wind speed v_{wind} $[m/s]$. Consider R as the turbine radius. Then,

$$\lambda = \frac{v_{tip}}{v_{wind}} = \frac{\omega_{turbine} R}{v_{wind}} \tag{3}$$

Then, the power extracted from the wind can be estimated by [2],

$$P_{wind} = \frac{1}{2} \rho A_{wt} C_p(\lambda, \theta) v_{wind}^3 \quad [W] \tag{4}$$

where ρ is the air density [kg/m^3], A_{wt} is the wind turbine swept area [m^2], v_{wind} is the wind speed [m/s] and C_p is the power coefficient. C_p is dimensionless and depends on both the *tip speed ratio*, λ, and the pitch angle, θ [degrees]. Note that C_p is lower than the Betz's limit, i.e., $\forall\ \lambda, \theta,\ C_p(\lambda, \theta) < 0.593$. Using a fixed pitch angle, typical power curves as a function of the wind speed and the turbine angular speed are depicted in Figure 2. Note that at every wind speed there is an optimum turbine speed at which the power extraction from the wind is maximized.

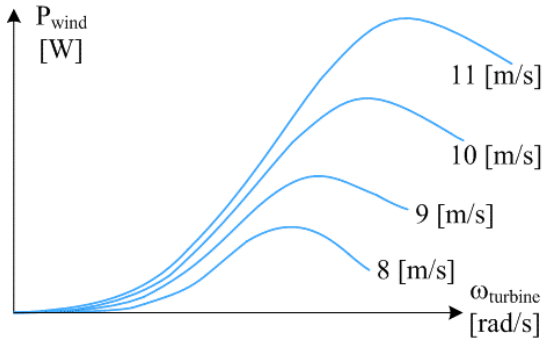

Figure 2. Extracted power from the wind.

III. DOUBLY-FED INDUCTION GENERATOR

By a proper adjustment of the voltage applied to the rotor circuits of the doubly-fed induction generator, the speed and consequently the active power can be controlled. Similarly, by adjusting the phase of the rotor voltages, the reactive power injected by the generator can be controlled. In order to understand these aspects, a steady-state machine representation is going to be derived from a fifth-order model.

A. Fifth-order model

Consider the following fifth-order differential-algebraic model of an induction machine [4].

$$\frac{1}{\omega_s} \frac{d\psi_{qs}}{dt} = V_{qs} + R_s I_{qs} - \psi_{ds} \tag{5}$$

$$\frac{1}{\omega_s}\frac{d\psi_{ds}}{dt} = V_{ds} + R_s I_{ds} + \psi_{qs} \quad (6)$$

$$\frac{1}{\omega_s}\frac{d\psi_{qr}}{dt} = V_{qr} - R_r I_{qr} - \frac{(\omega_s - \omega_r)}{\omega_s}\psi_{dr} \quad (7)$$

$$\frac{1}{\omega_s}\frac{d\psi_{dr}}{dt} = V_{dr} - R_r I_{dr} + \frac{(\omega_s - \omega_r)}{\omega_s}\psi_{qr} \quad (8)$$

$$\frac{2H}{\omega_s}\frac{d\omega_r}{dt} = T_m - T_e \quad (9)$$

$$\psi_{qs} = -X_s I_{qs} + X_m I_{qr} \quad (10)$$

$$\psi_{ds} = -X_s I_{ds} + X_m I_{dr} \quad (11)$$

$$\psi_{qr} = -X_m I_{qs} + X_r I_{qr} \quad (12)$$

$$\psi_{dr} = -X_m I_{ds} + X_r I_{dr} \quad (13)$$

where T_m is obtained dividing Equation (4) by $\frac{2}{p}\omega_r T_b$, where T_b is the machine torque base [5] and $T_e = \psi_{dr} I_{qr} - \psi_{qr} I_{dr}$. These equations are per-unitized and were obtained by assuming balanced operation and by using a synchronously rotating reference frame in which the *q-axis* leads the *d-axis* by 90°—electrical degrees. Generator convention is used, i.e., stator-currents are going out of the stator-circuits and rotor-currents are entering the rotor-circuits (see Figure 1). Equations (5)-(6) represent the stator-electrical dynamics, Equations (7)-(8) represent the rotor-electrical dynamics and Equation (9) models the mechanical motion of the machine shaft—typically known as swing equation. The constant H is obtained by representing the turbine, gearbox and machine shaft as a whole mass. Equations (10)-(13) are the machine flux-linkage equations. Note that $X_s = X_{\ell s} + X_m$ and $X_r = X_{\ell r} + X_m$ where $X_{\ell s}$ and $X_{\ell r}$ are the stator- and rotor-leakage reactance, respectively. If torsional-torque analysis is required, the swing equation can be replaced by a coupled multi-mass model, i.e., turbine, gearbox and induction-machine shaft are independently characterized by their mass [6]. Additionally, in general, the stator-electrical dynamics are faster compared to the rotor ones. Thus, a third-order dynamic model can be obtained by considering that stator variables can change instantaneously at any time [7,8], i.e., assuming an infinitely fast transient for the stator variables.

B. Steady-state equivalent model

Define the slip as $s = \frac{(\omega_s - \omega_r)}{\omega_s}$. When a synchronously rotating reference frame is used, all variables become constant at steady-state. Therefore, the machine steady-state equivalent circuit is obtained by setting the differential terms equal to zero. Substituting Equations (10)-(13) into Equations (5)-(8), the following steady-state equations are obtained.

$$V_{qs} = -R_s I_{qs} - X_s I_{ds} + X_m I_{dr} \quad (14)$$

$$V_{ds} = -R_s I_{ds} + X_s I_{qs} - X_m I_{qr} \quad (15)$$

$$\frac{V_{qr}}{s} = \frac{R_r}{s} I_{qr} - X_m I_{ds} + X_r I_{dr} \quad (16)$$

$$\frac{V_{dr}}{s} = \frac{R_r}{s} I_{dr} + X_m I_{qs} - X_r I_{qr} \quad (17)$$

Remember that the relation between the variables in the synchronously rotating reference frame and the variables in phasor representation is given by [4],

$$\overline{V}_{as} = V_{qs} - jV_{ds} : \text{Stator phasor voltage} \quad (18)$$

$$\overline{I}_{as} = I_{qs} - jI_{ds} : \text{Stator phasor current} \quad (19)$$

$$\overline{V}_{ar} = V_{qr} - jV_{dr} : \text{Rotor phasor voltage} \quad (20)$$

$$\overline{I}_{ar} = I_{qr} - jI_{dr} : \text{Rotor phasor current} \quad (21)$$

Thus, using Equations (14)-(21), the following equations are obtained.

$$\begin{aligned}\overline{V}_{as} &= V_{qs} - jV_{ds} \\ &= -R_s I_{qs} - X_s I_{ds} + X_m I_{dr} + jR_s I_{ds} - jX_s I_{qs} + jX_m I_{qr} \\ &= -(R_s + jX_s)(I_{qs} - jI_{ds}) + jX_m(I_{qr} - jI_{dr}) \\ &= -(R_s + jX_s)\overline{I}_{as} + jX_m\overline{I}_{ar} \quad (22)\end{aligned}$$

$$\begin{aligned}\frac{\overline{V}_{ar}}{s} &= \frac{V_{qr}}{s} - j\frac{V_{dr}}{s} \\ &= \frac{R_r}{s} I_{qr} - X_m I_{ds} + X_r I_{dr} - j\frac{R_r}{s} I_{dr} - jX_m I_{qs} + jX_r I_{qr} \\ &= (\frac{R_r}{s} + jX_r)(I_{qr} - jI_{dr}) - jX_m(I_{qs} - jI_{ds}) \\ &= (\frac{R_r}{s} + jX_r)\overline{I}_{ar} - jX_m\overline{I}_{as} \quad (23)\end{aligned}$$

Equations (22) and (23) define the steady model of the doubly-fed induction machine (see Figure 3).

C. Steady-state torque equation

By considering generator convention, the electromagnetic torque is defined as

$$\begin{aligned}T_e &= \psi_{dr} I_{qr} - \psi_{qr} I_{dr} \\ &= (-X_m I_{ds} + X_r I_{dr}) I_{qr} - (-X_m I_{qs} + X_r I_{qr}) I_{dr} \\ &= X_m(I_{qs} I_{dr} - I_{ds} I_{qr})\end{aligned}$$

$$= -X_m \Im(\overline{I}_{as}^* \overline{I}_{ar}) \tag{24}$$

where $\Im$ is imaginary part. By superposition theorem, $\overline{I}_{as}$ and $\overline{I}_{ar}$ can be calculated by independently considering the contribution of $\overline{V}_{as}$ and $\frac{\overline{V}_{ar}}{s}$ (see Figure 4). Thus, $\overline{I}_{as} = \overline{I}_{as}^{①} + \overline{I}_{as}^{②}$ and $\overline{I}_{ar} = \overline{I}_{ar}^{①} + \overline{I}_{ar}^{②}$. Then,

$$\overline{I}_{as}^{①} = \frac{-\overline{V}_{as}}{R_s + jX_{s\ell} + \frac{jX_m \frac{R_r}{s} - X_m X_{r\ell}}{\frac{R_r}{s} + jX_r}} \tag{25}$$

$$\overline{I}_{ar}^{①} = \frac{jX_m}{\frac{R_r}{s} + jX_r} \overline{I}_{as}^{①} \tag{26}$$

$$\overline{I}_{ar}^{②} = \frac{\frac{\overline{V}_{ar}}{s}}{\frac{R_r}{s} + jX_{r\ell} + \frac{jX_m R_s - X_m X_{s\ell}}{R_s + jX_s}} \tag{27}$$

$$\overline{I}_{as}^{②} = \frac{jX_m}{R_s + jX_s} \overline{I}_{ar}^{②} \tag{28}$$

Therefore, the torque expression becomes,

$$\begin{aligned} T_e &= -X_m \Im(\overline{I}_{as}^* \overline{I}_{ar}) \\ &= -X_m \Im(\overline{I}_{as}^{①*} \overline{I}_{ar}^{①}) - X_m \Im(\overline{I}_{as}^{①*} \overline{I}_{ar}^{②} + \overline{I}_{as}^{②*} (\overline{I}_{ar}^{①} + \overline{I}_{ar}^{②})) \\ &= \frac{-X_m^2 \frac{R_r}{s}}{\frac{R_r^2}{s^2} + X_r^2} |\overline{I}_{as}^{①}|^2 \\ &\quad - X_m \Im(\overline{I}_{as}^{①*} \overline{I}_{ar}^{②} + \overline{I}_{as}^{②*} (\overline{I}_{ar}^{①} + \overline{I}_{ar}^{②})) \end{aligned} \tag{29}$$

The first term on the right-hand side is the same expression for the torque of an induction machine with short-circuited rotor windings [4]. The second term is the torque component related to the rotor voltages.

D. Alternative way to calculate the electrical torque from the equivalent circuit

Consider the voltage polarity and current directions defined in Figure 3. Then, the active power that crosses the airgap is the power injected by the source $\frac{\overline{V}_{ar}}{s}$ minus the losses in the resistor $\frac{R_r}{s}$.

$$P_{airgap} = \Re\left(\frac{\overline{V}_{ar}}{s} \overline{I}_{ar}^*\right) - \frac{R_r}{s} |\overline{I}_{ar}|^2 \tag{30}$$

where $\Re$ is real part. On the other hand, physically, the power that crosses the airgap is the mechanical power from the shaft plus the power injected to the slip rings minus the rotor losses [9]. Thus,

$$P_{airgap} = P_{mec} + \Re\left(\overline{V}_{ar} \overline{I}_{ar}^*\right) - R_r |\overline{I}_{ar}|^2 \tag{31}$$

Comparing equations (30) and (31), the following expression for the mechanical power is obtained.

$$P_{mec} = \left\{P_r - R_r |\overline{I}_{ar}|^2\right\} \frac{(1-s)}{s} \tag{32}$$

where $P_r = \Re(\overline{V}_{ar} \overline{I}_{ar}^*)$. A modified equivalent circuit is presented in Figure 5 to represent the mechanical power and the power injected by the rotor-side converter. Note that by energy conservation, $P_{mec} + P_r - P_{losses} = P_s \Rightarrow P_{gen} = P_s - P_r = P_{mec} - P_{losses}$.

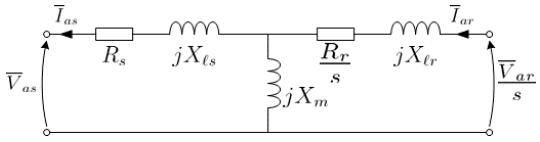

Figure 3. Steady-state equivalent circuit of the doubly-fed induction machine.

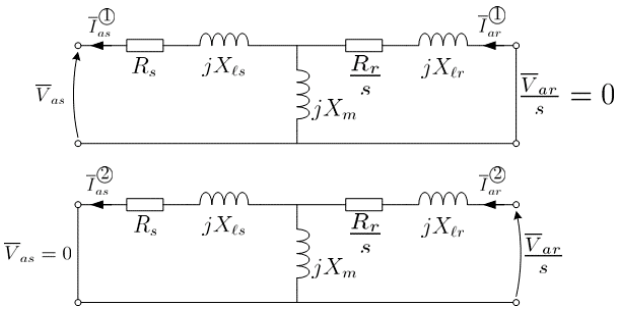

Figure 4. Superposition theorem applied to the equivalent circuit of the doubly-fed induction machine.

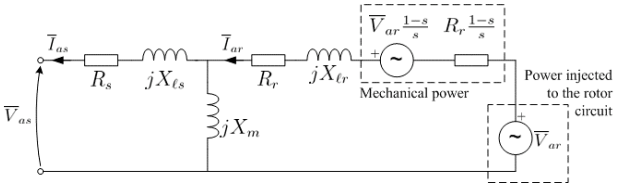

Figure 5. Modified equivalent circuit of the doubly-fed induction machine.

Using Equation (32), the electrical torque is defined by

$$T_e = \frac{P_{mec}\ [pu]}{w_{shaft}\ [pu]} = \frac{\left\{P_r - R_r |\overline{I}_{ar}|^2\right\}}{s} \tag{33}$$

The efficiency (η) of the doubly-fed induction machine depends on whether the machine is acting as a generator or as a motor. As a generator, $|P_{gen}| \leq |P_{mec}|$. As a motor, $|P_{gen}| > |P_{mec}|$. Neglecting mechanical and stator losses, the efficiency in generator mode is

$$\eta_{gen} = \frac{P_{gen}}{P_{mec}} = \frac{P_s}{P_r} = \frac{P_{mec} - P_{losses}}{P_{mec}} = \frac{P_r \frac{(1-s)}{s} - R_r \left|\overline{I}_{ar}\right|^2 \frac{1}{s}}{\left(P_r - R_r \left|\overline{I}_{ar}\right|^2\right) \frac{(1-s)}{s}} \quad (34)$$

For the particular case when the rotor circuit is short-circuited, i.e., $\overline{V}_{ar} = 0$ as an induction machine,

$$\eta_{gen} = \frac{P_{gen}}{P_{mec}} = \frac{1}{(1-s)} \quad (35)$$

When the doubly-fed induction machine is acting as a motor, the efficiency is $\eta_{motor} = \frac{P_{mec}}{P_{gen}} = \eta_{gen}^{-1}$.

E. Active and reactive power output

In order to understand the effect of the rotor voltages, the active and reactive power given by the generator is obtained for two cases. In the first one, assume that $V_{dr} = 0$ while V_{qr} is varied from -0.04 to $+0.04$ [pu]. In the second one, assume that $V_{qr} = 0$ while V_{dr} is varied from -0.04 to $+0.04$ [pu]. Consider $X_{\ell s} = 0.03$, $X_{\ell r} = 0.08$, $X_m = 3$ and $R_s = R_r = 0.01$ (all quantities are in per unit). Note that the total active power injected by the generator to the grid is defined as $P_{gen} = P_s - P_r$, where P_s is the active power going out of the stator and P_r is the active power absorbed by the rotor. Note that the grid- and rotor-side converters and the *DC*-link are assumed to be lossless. On the other hand, the reactive power injected by the generator to the grid is defined as $Q_{gen} = Q_s$, where Q_s is the reactive power going out of the stator. Note that this assumes that the reactive power absorbed by the rotor circuit is given by the rotor-side converter and the grid-side converter is operated at unity power factor [10].

Figures 6 and 7 show the results. Notice that solid-, dotted- and dashed-line correspond to positive, zero and negative voltages, respectively. In the stable-region of the power characteristic—region where the derivative of the power with respect to the slip is negative—, increasing values of V_{qr} shift the active-power curve upwards and the reactive-power curve to the right (Figure 6), i.e., more active power is injected to the grid but the machine reactive-power absorption is increased in generator mode. On the other hand, increasing values of V_{dr} raise the negative active-power-curve slope and shift the reactive-power curve upwards (Figure 7), i.e., considerable reactive power is injected to the grid and the active-power is slightly increased in generator mode. These results show the capability of the machine to give reactive-power support. Additionally, it is evident a strong coupling in both pairs (P_{gen}, V_{qr}) and (Q_{gen}, V_{dr}) and a weak coupling in (P_{gen}, V_{dr}) and (Q_{gen}, V_{qr}). The design of doubly-fed induction-machine controllers are based on these coupling characteristics.

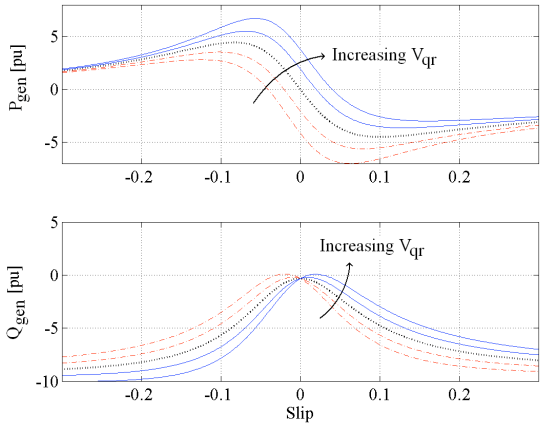

Figure 6. P_{gen} and Q_{gen} as a function of the slip and the voltage V_{qr} (note that $V_{dr} = 0$)

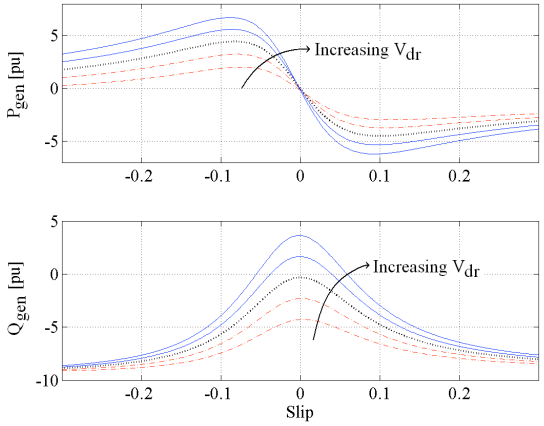

Figure 7. P_{gen} and Q_{gen} in function of the slip and the voltage V_{dr} (note that $V_{qr} = 0$)

F. PQ capability

The reactive-power capability of a doubly-fed induction machine presents similarities to the conventional synchronous generator capability. It depends on the active-power generated, the slip and the limitations due to stator and rotor maximum-currents as well as the maximum rotor voltage [11,12]. In order to understand the power capability curve, the following circuital relationships are obtained from the equivalent circuit (Figure 3).

$$\begin{bmatrix}\overline{V}_{as}\\ \frac{\overline{V}_{ar}}{s}\end{bmatrix} = \underbrace{\begin{bmatrix}-(R_s+jX_s) & jX_m\\ -jX_m & \frac{R_r}{s}+jX_r\end{bmatrix}}_{Z}\begin{bmatrix}\overline{I}_{as}\\ \overline{I}_{ar}\end{bmatrix} \tag{36}$$

$$\begin{bmatrix}\overline{I}_{as}\\ \overline{I}_{ar}\end{bmatrix} = Y\begin{bmatrix}\overline{V}_{as}\\ \frac{\overline{V}_{ar}}{s}\end{bmatrix}, \quad Y = Z^{-1} \tag{37}$$

$$\begin{bmatrix}\overline{I}_{as}\\ \frac{\overline{V}_{ar}}{s}\end{bmatrix} = \underbrace{\begin{bmatrix}\frac{-1}{R_s+jX_s} & \frac{jX_m}{R_s+jX_s}\\ \frac{jX_m}{R_s+jX_s} & \frac{R_r}{s}+jX_r+\frac{X_m^2}{R_s+jX_s}\end{bmatrix}}_{G}\begin{bmatrix}\overline{V}_{as}\\ \overline{I}_{ar}\end{bmatrix} \tag{38}$$

$$\begin{bmatrix}\frac{\overline{V}_{ar}}{s}\\ \overline{I}_{ar}\end{bmatrix} = \underbrace{\begin{bmatrix}\frac{\frac{R_r}{s}+jX_r}{jX_m} & \frac{\left(\frac{R_r}{s}+jX_r\right)(R_s+jX_s)+X_m^2}{jX_m}\\ \frac{1}{jX_m} & \frac{R_s+jX_s}{jX_m}\end{bmatrix}}_{B}\begin{bmatrix}\overline{V}_{as}\\ \overline{I}_{as}\end{bmatrix} \tag{39}$$

1. Maximum rotor current

Considering that the converters and the *DC*-link are lossless and the grid-side converter is typically operated at unity power factor, the total power injected by the doubly-fed induction generator is $\overline{S}_{gen} = \overline{S}_s - \Re\{\overline{S}_r\}$ where $\overline{S}_s$ is the complex-power going out of the stator and $\overline{S}_r$ is the complex-power going into the rotor. Using Equation (38), these powers are defined by,

$$\begin{aligned}\overline{S}_s &= \overline{V}_{as}\overline{I}_{as}^* = \overline{V}_{as}(G_{11}\overline{V}_{as}+G_{12}\overline{I}_{ar})^*\\ &= \frac{-1}{R_s-jX_s}\left|\overline{V}_{as}\right|^2 + \frac{-jX_m}{R_s-jX_s}\overline{V}_{as}\overline{I}_{ar}^*\end{aligned} \tag{40}$$

$$\begin{aligned}\overline{S}_r &= \overline{V}_{ar}\overline{I}_{ar}^* = s(G_{21}\overline{V}_{as}+G_{22}\overline{I}_{ar})\overline{I}_{ar}^*\\ &= \frac{s\ jX_m}{R_s+jX_s}\overline{V}_{as}\overline{I}_{ar}^* + s\left(\frac{R_r}{s}+jX_r+\frac{X_m^2}{R_s+jX_s}\right)\left|\overline{I}_{ar}\right|^*\end{aligned} \tag{41}$$

Typically, $R_s \ll X_m < X_s$ and $R_r \ll X_m < X_r$. Thus, the real part of the second term on the right-hand side of Equation (42) may be neglected. It turns out that $P_r = \Re(\overline{S}_r) \approx s\Re(\overline{S}_s) = sP_s$. In Figure 8, a scheme of the active-power balance under super- and sub-synchronous speed is presented. P_{mec} corresponds to the mechanical power sent into the machine shaft by the wind turbine. Note that the imaginary part of Equation (41), which corresponds to the reactive power injected to the rotor, is supplied by the rotor-side converter instead of the grid. In summary, $\overline{S}_{gen} = \overline{S}_s - sP_s$.

Assuming $\overline{V}_{as} = V_s e^{j0}\ [pu]$, $\overline{I}_{ar} = I_r e^{-j\theta}$ and $R_s \ll X_s$, a simplified expression for the complex power injected by the generator is obtained as follow.

$$\begin{aligned}\overline{S}_{gen} &\approx \frac{1}{jX_s}\left|\overline{V}_{as}\right|^2 + \frac{X_m}{X_s}\overline{V}_{as}\overline{I}_{ar}^* - s\Re\overline{S}_s\\ &\approx \frac{\left|\overline{V}_{as}\right|^2}{jX_s} + \frac{X_m}{X_s}\overline{V}_{as}\overline{I}_{ar}^* - s\Re\left\{\frac{X_m}{X_s}\overline{V}_{as}\overline{I}_{ar}^*\right\}\\ &= -j\frac{V_s^2}{X_s} + (1-s)\frac{X_m}{X_s}V_sI_r\cos\theta + j\frac{X_m}{X_s}V_sI_r\sin\theta\end{aligned} \tag{42}$$

Equation (42) represents an ellipsoid with center at $-j\frac{V_s^2}{X_s}$ in the $P-Q$ plane. If $I_r = I_r^{max}$, then this ellipsoid defines the boundary of a safe operation.

2. Maximum rotor-voltage and stator-current

Similar to the maximum rotor-current limitation, boundaries of a safe operation can be found by considering a maximum rotor-voltage and maximum stator-current. For maximum rotor-voltage it is required to find an expression between power and rotor-voltage. Use Equation (37) to obtain,

$$\overline{S}_s = \overline{V}_{as}\overline{I}_{as}^* = \overline{V}_{as}\left(Y_{11}\overline{V}_{as}+Y_{12}\frac{\overline{V}_{ar}}{s}\right)^* \tag{43}$$

$$\overline{S}_r = \overline{V}_{ar}\overline{I}_{ar}^* = \overline{V}_{ar}\left(Y_{21}\overline{V}_{as}+Y_{22}\frac{\overline{V}_{ar}}{s}\right)^* \tag{44}$$

For stator-current, an expression between power and stator-current is required. Use Equation (39) to obtain,

$$\overline{S}_s = \overline{V}_{as}\overline{I}_{as}^* \tag{45}$$

$$\begin{aligned}\overline{S}_r &= \overline{V}_{ar}\overline{I}_{ar}^*\\ &= s\left(B_{11}\overline{V}_{as}+B_{12}\overline{I}_{as}\right)\left(B_{21}\overline{V}_{as}+B_{22}\overline{I}_{as}\right)^*\end{aligned} \tag{46}$$

For each case compute $S_{gen} = \overline{S}_s - \Re(\overline{S}_r)$. In Figure 9, the capability curve for a super-synchronous and a sub-synchronous speed is presented. The same parameters used in Section III-E are considered. Among the three limits described above, at every point the lowest one is used to create the capability curve (thick solid line).

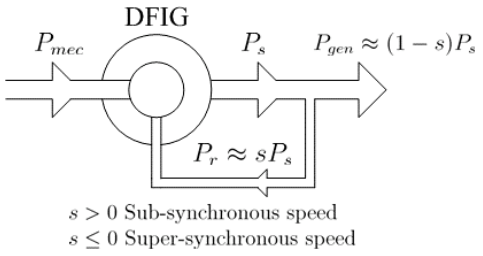

Figure 8. Active-power flows in the doubly-fed induction machine.

IV. CONCLUSIONS

This paper presents the steady-state model of a doubly-fed induction generator used in variable-speed wind power generation. Using a fifth order dynamic model of an induction machine, a well-known modified equivalent circuit is derived from which the machine torque equation can be easily obtained. It uses a synchronously rotating reference frame in which the *q-axis* leads the *d-axis* by ninety degrees, In addition, the relationships between power and rotor-voltages are analyzed. A strong coupling in the q-axis rotor voltage and active power as well as the d-axis rotor voltage and reactive power is observed. When the q-axis rotor voltage is increased, the active power characteristic is shifted upwards on the stable zone, i.e., more active power is generated, however, more reactive power is absorbed by the machine. On the other hand, when the d-axis rotor voltage is increased, the reactive power characteristic is shifted upwards, either more reactive-power is injected to the grid or the reactive power absorption is decreased. In this case, a slight increase of the injected active power is observed in generator mode. In general, there is a weak coupling in both d-axis rotor voltage and active power as well as q-axis rotor voltage and reactive power. Finally, the machine capability to give reactive power support is discussed. The power capability characteristic of the machine is described which shows similarities to the capability curve of conventional synchronous generators.

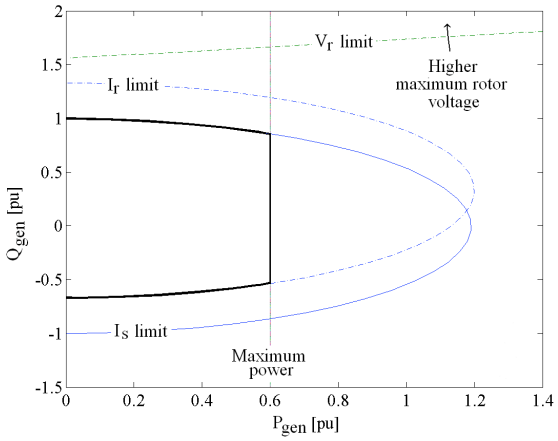

(a)

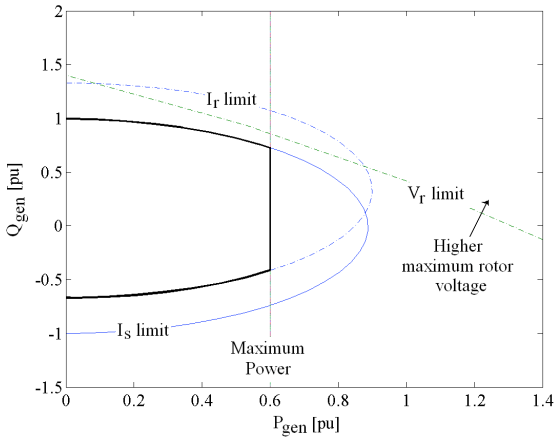

(b)

Figure 9. Power capability of a doubly-fed induction generator: (a) Super-synchronous speed with $V_s = 1$ [pu], $s = -0.2$, $I_s^{max} = 1$ [pu], $I_r^{max} = 1$ [pu], $V_r^{max} = 0.24$ [pu] and $P^{max} = 0.6$ [pu], (b) Sub-synchronous speed with $V_s = 1$ [pu], $s = 0.1$, $I_s^{max} = 1$ [pu], $I_r^{max} = 1$ [pu], $V_r^{max} = 0.12$ [pu] and $P^{max} = 0.6$ [pu].

REFERENCES

1. Z. Saad-Saoud, N. Jenkins, "Simple wind farm dynamic model," *IEE Proceedings: Generation, Transmission and Distribution*, vol.142, no.5, pp.545-548, 1995.

2. T. Ackermann, *Wind power in power systems*, John Wiley and Sons, Ltd., 2005.

3. R. Scherer, "Blade design aspects," *Renewable Energy*, vol.16, pp.1272-1277, 1999.

4. P.C. Krause, O. Wasynczuk, S.D. Sudhoff, *Analysis of Electric Machinery and Drive Systems*, Wiley-IEEE Press, 2nd ed., 2002.

5. H.A. Pulgar-Painemal, P.W. Sauer, "Dynamic modeling of wind power generation," North American Power Symposium, Mississippi, 2009.

6. D. Stojanovic, D. Petrovic, N. Mitrovic, "Analysis of torsional torques of big turbine-generator shafts," *International Conference on Power System Transients*, Budapest, Hungary, pp.301-306, 1999.

7. S. Ahmed-Zaid, M. Taleb, "Structural modeling of small and large induction machines using integral manifolds," IEEE Transactions on Energy Conversion, vol.6, no.3, pp.529-535, 1991.

8. E. Drennan, S. Ahmed-Zaid, P.W. Sauer, "Invariant manifolds and start-up dynamics of induction machines," North American Power Symposium, Missouri, 1989.

9. L. Jiao, Boon-Teck Ooi, G. Joos, F. Zhou, "Doubly-fed induction generator (DFIG) as a hybrid of asynchronous and synchronous machines," *Electric Power Systems Research*, vol.76, pp.33-37, 2005.

10. V. Akhmatov, "Variable-speed wind turbines with doubly-fed induction generators. Part III: Model with the back-to-back converters," *Wind Engineering*, vol.27, no.2, pp.79-91, 2003.

11. T. Lund, P. Sorensen, "Reactive power capability of a wind turbine with doubly fed induction generator," *Wind Energy*, vol.0, pp.379-394, 2007.

12. D. Santos-Martin, S. Arnaltes, J.L. Rodriguez-Amenedo, "Reactive power capability of doubly fed asynchronous generators," *Electric Power Systems Research*, vol.78, pp.1837-1840, 2008.

Hector A. Pulgar-Painemal received the BS and MS degrees in Electrical Engineering from Concepcion University, Chile, in 2001 and 2003, respectively. Since 2003, he has been an Academic Instructor at the Technical Federico Santa Maria University, Chile. Currently, he is a Ph.D. student at the University of Illinois at Urbana Champaign. His areas of interest are systems dynamics, stability, operation and planning of power systems.

Peter W. Sauer received the B.S. degree in electrical engineering from the University of Missouri at Rolla in 1969, and the M.S. and Ph.D. degrees in electrical engineering from Purdue University, Lafayette, IN, in 1974 and 1977, respectively. He has been on the faculty at the University of Illinois at Urbana-Champaign since 1977 where he teaches courses and directs research on power systems and electric machines.